Propagation of small size magnetic holes in the magnetospheric plasma sheet

S. T. Yao, Q. Q. Shi, Z. Y. Li, X. G. Wang, A. M. Tian, W. J. Sun, M. Hamrin, M. M. Wang, T. Pitkänen, S. C. Bai, et al.

AGU PUBLICATIONS

JGR

Journal of Geophysical Research: Space Physics

RESEARCH ARTICLE
10.1002/2016JA022741

Key Points:
- The velocity of small size magnetic holes in the plasma flow is calculated
- The results show that they are propagating in the plasma flow
- The structure velocity agrees with the electron soliton velocity

Correspondence to:
Q. Q. Shi and A. M. Tian,
sqq@sdu.edu.cn;
Tianam@sdu.edu.cn

Citation:
Yao, S. T., et al. (2016), Propagation of small size magnetic holes in the magnetospheric plasma sheet, *J. Geophys. Res. Space Physics*, *121*, 5510–5519, doi:10.1002/2016JA022741.

Received 25 MAR 2016
Accepted 3 JUN 2016
Accepted article online 7 JUN 2016
Published online 30 JUN 2016

Propagation of small size magnetic holes in the magnetospheric plasma sheet

S. T. Yao[1], Q. Q. Shi[1], Z. Y. Li[2], X. G. Wang[3], A. M. Tian[1], W. J. Sun[4], M. Hamrin[5], M. M. Wang[1], T. Pitkänen[5], S. C. Bai[1], X. C. Shen[1], X. F. Ji[2], D. Pokhotelov[6], Z. H. Yao[6], T. Xiao[1], Z. Y. Pu[4], S. Y. Fu[4], Q. G. Zong[4], A. De Spiegeleer[5], W. Liu[7], H. Zhang[8,9], and H. Rème[10,11]

[1]Shandong Provincial Key Laboratory of Optical Astronomy and Solar-Terrestrial Environment, Institute of Space Sciences, Shandong University, Weihai, China, [2]State Key Laboratory of Nuclear Physics and Technology, School of Physics, Peking University, Beijing, China, [3]Department of Physics, Harbin Institute of Technology, Harbin, China, [4]School of Earth and Space Sciences, Peking University, Beijing, China, [5]Department of Physics, Umeå University, Umeå, Sweden, [6]Mullard Space Science Laboratory, University College London, London, UK, [7]School of Space and Environment, Beihang University, Beijing, China, [8]Key Laboratory of Earth and Planetary Physics, Institute of Geology and Geophysics, Chinese Academy of Sciences, Beijing, China, [9]Beijing National Observatory of Space Environment, Institute of Geology and Geophysics, Chinese Academy of Sciences, Beijing, China, [10]University of Toulouse, UPS-OMP, IRAP, Toulouse, France, [11]CNRS, IRAP, Toulouse, France

Abstract Magnetic holes (MHs), characteristic structures where the magnetic field magnitude decreases significantly, have been frequently observed in space plasmas. Particularly, small size magnetic holes (SSMHs) which the scale is less than or close to the proton gyroradius are recently detected in the magnetospheric plasma sheet. In this study of Cluster observations, by the timing method, the minimum directional difference (MDD) method, and the spatiotemporal difference (STD) method, we obtain the propagation velocity of SSMHs in the plasma flow frame. Furthermore, based on electron magnetohydrodynamics (EMHD) theory we calculate the velocity, width, and depth of the electron solitary wave and compare it to SSMH observations. The result shows a good accord between the theory and the observation.

1. Introduction

Magnetic holes (MHs), structures of a significant magnetic field magnitude decrease, have been widely observed in space plasmas [e.g., *Turner et al.*, 1977; *Winterhalter et al.*, 1994; *Tsurutani et al.*, 2009; *Shi et al.*, 2009a; *Xiao et al.*, 2010; *Sun et al.*, 2012]. Previous studies have associated MHs, detected in the solar wind and in the planetary magnetosheath/cusp, with mirror instabilities [e.g., *Kaufmann et al.*, 1970; *Tsurutani et al.*, 1982; *Southwood and Kivelson*, 1993; *Fazakerley and Southwood*, 1994; *Chisham et al.*, 1999; *Horbury et al.*, 2004; *Joy et al.*, 2006; *Zhang et al.*, 2008, 2009; *Shi et al.*, 2009a; *Xiao et al.*, 2010, 2011, 2014]. However, there are still several candidates for MHs formation, such as soliton waves [*Baumgärtel*, 1999; *Stasiewicz*, 2004] and sheet-like equilibrium structures [*Burlaga and Lemaire*, 1978]. The wide scale range of MHs, from several to thousands of ion gyroradius, accompanied by different background plasma features, strongly indicates that the structures are formed by various mechanisms; and thus, alternative approaches are required [*Tsurutani et al.*, 2011].

Small size magnetic holes (SSMHs), also in the name of "subproton-scale magnetic holes" [*Sundberg et al.*, 2015] are structures with a scale less than, or close to, the proton gyroradius. In recent years, this kind of structures has been frequently observed by the Time History of Events and Macroscale Interactions during Substorms and the Cluster satellites in the magnetospheric plasma sheet [*Ge et al.*, 2011; *Sun et al.*, 2012]. SSMHs reported by *Ge et al.* [2011] were found to be quite different from those reported by *Sun et al.* [2012]. The former were detected in a perturbed magnetotail, and the latter were more frequently observed in a quiet magnetotail. The tearing structure was suggested by *Balikhin et al.* [2012] to account for the observation of *Ge et al.* [2011], and the electron solitary wave [*Ji et al.*, 2014] was proposed for the mechanism of SSMHs observed by *Sun et al.* [2012]. By including the anisotropy of the electron pressure tensor to take the Biermann battery effect into account [*Biermann*, 1950], a Korteweg-deVries equation in modified electron magnetohydrodynamics (EMHD) was developed to obtain the solution of the one-dimensional (1-D) slow-mode soliton [*Ji et al.*, 2014]. The solution showed a good agreement with the observation of *Sun et al.* [2012]. *Sundberg et al.* [2015] further discussed various possible generation mechanisms of SSMHs in the plasma sheet, including ion or electron mirror modes and field-swelling instabilities [e.g., *Basu and*

Coppi, 1982; *Gary and Karimabadi*, 2006; *Pokhotelov et al*., 2013], tearing modes [*Balikhin et al*., 2012], electron vortices [*Haynes et al*., 2015], and solitary waves [e.g., *Baumgärtel*, 1999; *Stasiewicz et al*., 2003; *Stasiewicz*, 2004; *Ji et al*., 2014], and suggested the tearing mode, the electron vortex, and the solitary waves were candidates for the SSMHs formation in the plasma sheet.

In this article, we further report observations of a series of SSMHs propagating in the plasma sheet. The timing method [*Russell et al*., 1983], the minimum directional difference (MDD) method [*Shi et al*., 2005], and the spatiotemporal difference (STD) method [*Shi et al*., 2006] are used to calculate the velocity of SSMHs. Also, based on the EMHD model of *Ji et al*. [2014], we calculate the velocity of the 1-D slow-mode electron solitary wave and compare it with the velocity of SSMHs in the plasma sheet. The layout of the paper is as follows. We first introduce the data set and analysis methods in section 2 and then calculate the velocity of SSMHs with the different methods in section 3. A comparison between the theory and the SSMHs velocity data in the plasma sheet is shown in section 4. The paper is summarized then in section 5.

2. Data Analysis and Methods

2.1. Event Selection

We use the Fluxgate Magnetometer (FGM) [*Balogh et al*., 2001] instrument on board all four Cluster spacecraft to obtain high-resolution magnetic field data (5 samples per second). We also use the Hot Ion Analyzer (HIA) of the Cluster Ion Spectrometry (CIS) instrument [*Rème et al*., 2001] on board Cluster C1 to obtain velocity data of a 4 s resolution, and the Plasma Electron and Current Experiment (PEACE) [*Johnstone et al*., 1997] instrument on board Cluster C1–C4 to obtain electron density data (0.25 samples per second).

All SSMHs studied herein are selected from *Sun et al*. [2012] of 72 events observed by Cluster and identified in the procedure of *Zhang et al*. [2008] with $B_{min}/B \leq 0.75$, $\omega \leq 15°$, where B_{min} and B are, respectively, the minimum and average magnetic field magnitudes within a sliding window of 300 s, and ω is the angle between the starting and ending vectors closest to the two MH boundaries, indicating the direction change of the magnetic field over the event. Here the boundary is considered as the edge where magnetic field intensity begins to decrease to $(B - \delta)$ (δ is the standard deviation of magnetic field in the 300 s window). The 72 events can be sorted into two classes [*Ji*, 2015]. The criteria for class I are the following: (1) the structure is detected by at least three satellites, and (2) at least three spacecraft are in the plane perpendicular to the magnetic field maximum variation direction. In the 72 events, 39 satisfy the above criteria. The other 33 events are then sorted as class II. The class I MHs can further sorted into two groups: 1-D structures (16 events) and other structures (23 events). The identification of 1-D structures can be described as follows: (1) all four Cluster spacecraft (C1–C4) must detect a magnetic field dip; (2) for such a structure, if $(b_{max} - b_{min})/b_{max} \leq 30\,\%$, it is then considered as 1-D, where b_{max} and b_{min} are, respectively, the maximum and minimum among the individual minimum magnetic field reading of each Cluster spacecraft. It is well known that the timing method (introduced in section 2.2) works well for 1-D structures. However, the accuracy of the results strongly depends on the profile of the observed magnetic field [*Russell et al*., 1983]. Thus, the identification of 1-D structures should be done more carefully. The ideal situation is that the 1-D MH magnetic field signatures have the same shape and depth for all four spacecraft, showing clear boundaries (observed by the four spacecraft at respective moments). With this requirement, ten 1-D events (from July 2003 to October 2003, observed in the nightside central plasma sheet) are selected and then investigated in detail in this article. The process of event selection is shown in Figure 1.

2.2. Timing Method

The timing method [see *Russell et al*., 1983; *Paschmann et al*., 1998] has a wide applicability in practice. It has been used to determine the normal direction and velocity of the bow shock and interplanetary shocks [e.g., *Russell et al*., 1983; *Schwartz*, 1998]. The Cluster mission makes it possible to determine the normal direction and velocity of the boundary of MHs where sharp changes in the magnitude of the magnetic field are observed. *Knetter et al*. [2004] investigated discontinuities in the solar wind by using multipoint Cluster data. A useful method for determining the error of the timing method was also presented in *Knetter et al*. [2004] and *Knetter* [2005]. In this study, a similar method is used to calculate the velocity and normal direction of

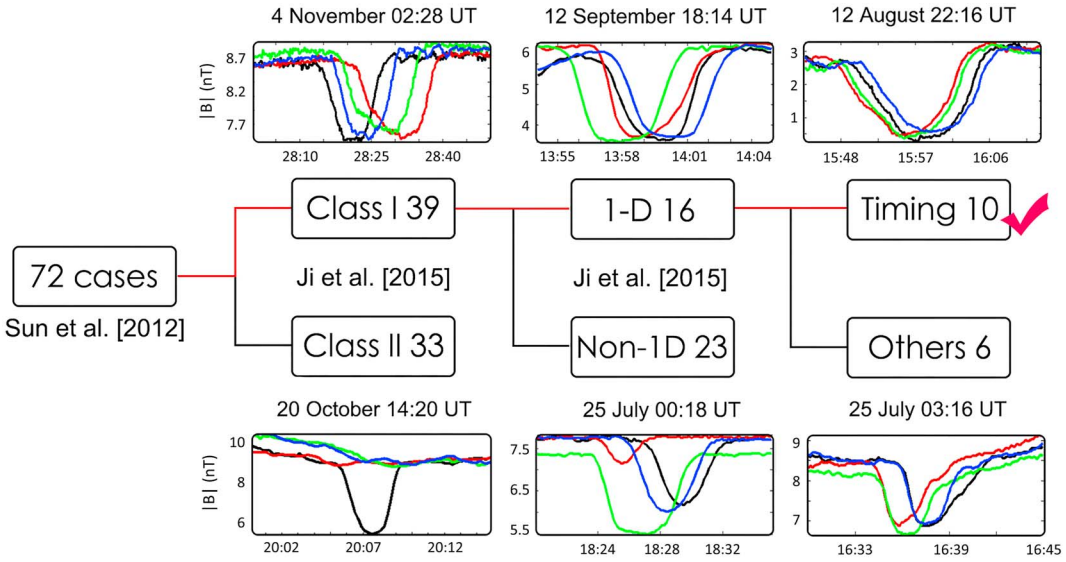

Figure 1. Selection process for events observed in 2003. Six examples are plotted, with the black, red, green, and blue curves for magnetic field magnitudes observed by four Cluster spacecraft, respectively.

the boundary of MHs from Cluster magnetic field measurements. The basic equation of timing analysis is as follows:

$$U\left(t_i - t_j\right) = \left(\mathbf{r_i} - \mathbf{r_j}\right)\cdot\mathbf{n}. \tag{1}$$

Here $\mathbf{n}$ and U are the unit normal vector of the MH boundary and the velocity along the normal direction, respectively. And $|\mathbf{r_i} - \mathbf{r_j}|$ is the distance between two spacecraft (i and j) observing the same boundary of an MH (other parameters, e.g., density, temperature, flux etc. can also be used), as seen in the magnetic field data in this article. If a structure first encounters C1, and then C2–C4, we consider C1 as the reference satellite, and then the interspacecraft distance $|\mathbf{r_1} - \mathbf{r_j}|$ and the corresponding time interval $\Delta t = t_1 - t_j$ between C1 and the other three spacecraft can be obtained. By solving the system of equation (1) for all four spacecraft pairs, we obtain U and $\mathbf{n}$. The uncertainty of U comes from errors in time delays and distances between different spacecraft pairs. Since the position has much higher precision, the uncertainty in the relative timing is thus the main error source. An empirical range of the timing error, $\delta t = 0.1\Delta t$, was used in *Knetter et al.* [2004]. Different shapes of the magnetic field magnitude curves can also contribute uncertainty to the results. One can define an interval $[\Delta t - \delta t, \Delta t + \delta t]$ and mark 11 equidistant samples in it [*Knetter*, 2005]. Therefore Δt is extended to a vector, e.g., $\left[\Delta t - \delta t,\ \Delta t - \frac{4}{5}\delta t,\ \Delta t - \frac{3}{5}\delta t,\ \Delta t - \frac{2}{5}\delta t,\ \Delta t - \frac{1}{5}\delta t,\ \Delta t,\ \Delta t + \frac{1}{5}\delta t,\ \Delta t + \frac{2}{5}\delta t,\ \Delta t + \frac{3}{5}\delta t,\ \Delta t + \frac{4}{5}\delta t,\ \Delta t + \delta t\right]$. As four spacecraft (three spacecraft pairs) determine three relative time intervals, a total of 11^3 combinations of time intervals can be produced. By solving the set of equation (1), 11^3 velocities and normal directions can be obtained. According to the result, the mean propagation velocity and normal direction can be calculated and the standard deviations are regarded as the uncertainty of the timing velocity. An explicit example is shown in subsection 3.1.

2.3. Time-Varying Dimensionality and Velocity Determination Methods: MDD and STD

The minimum directional derivative (MDD) method [*Shi et al.*, 2005] has been widely used to determine the structural dimensionality and the principal directions by calculating the eigenvalues and eigenvectors of $L = \left(\nabla \vec{B}\right)\left(\nabla \vec{B}\right)^T$, where T denotes transpose by using multipoint data [e.g., *Shi et al.*, 2009a, 2009b, 2013; *Denton et al.*, 2010, 2012; *Sun et al.*, 2010; *Wendel and Adrian*, 2013]. This method provides three normal orientations, respectively, corresponding to the direction of maximum, minimum, and intermediate magnetic field variations. Previous studies show that this method is effective and useful for obtaining the normal axis orientation of 1-D structures such as discontinuities or determining the invariant directions for 2-D structures such as flux tubes [*Shi et al.*, 2005]. One of the notable points is that the method calculates the direction temporally and makes it possible to study the evolution of the principal direction.

Furthermore, with the spatial-temporal difference (STD) method [*Shi et al.*, 2006] one can calculate the velocity of quasi-stationary structures from multipoint data measurements of the magnetic field temporally by solving the equation of $\frac{\partial \vec{B}}{\partial t} + \vec{V}_{str} \cdot \nabla \vec{B} = 0$, where $\vec{V}_{str}$ is the velocity of the structure in the satellite reference frame, $\vec{B}$ is the magnetic field, and t is the time. The solution is obtained and projected onto the maximum and intermediate directions from the MDD method. Therefore, a velocity vector in the maximum and intermediate directions can be obtained. The advantage of the STD method is that, whatever the dimensionality of the structure is, the velocity can be calculated directly. Similar to the MDD method, the temporal variation of the velocity can be studied with the STD method due to the relative motion of the structures with respect to the spacecraft.

3. Propagating Properties of SSMHs

In section 3, the velocity vectors of the selected SSMHs are calculated by the timing method. Since this method can only be applied to 1-D structures, the MDD method is used to examine the dimensionality of the SSMHs. Thereafter, the normal direction and the velocity of the SSMHs are obtained again by the MDD and STD methods, respectively. We compare the results from the timing, and the MDD and STD methods at the end of this section.

3.1. Timing Analysis

We first calculate the timing velocity for the selected SSMHs in the satellite frame and in the plasma flow frame, respectively. The velocity in the plasma flow frame, U_p, is obtained by

$$U_p = U - \vec{\mathbf{V}} \cdot \vec{\mathbf{n}} . \tag{2}$$

Here U is the timing velocity obtained by equation (1) from magnetic field data, and $\vec{\mathbf{V}}$ is the background plasma flow velocity obtained as a 1 min average from CIS-HIA ion moments. The GSE coordinate system is used. If the error bar of the resulting U_p crosses zero, we consider this event to be "frozen" in the plasma flow since it is very likely that $U_p = 0$. And in the other case, if U_p is far from zero, we conclude that the MH is propagating relative to the plasma flow. On the basis of equation (2), we provide a comprehensive uncertainty analysis. The uncertainty of U_p comes from U, $\vec{\mathbf{V}}$, and $\vec{\mathbf{n}}$. We consider a CIS-HIA instrument uncertainty of 10% in the magnitude of $\vec{\mathbf{V}}$ and 5° in the velocity direction [*Rème et al.*, 2001]. Using these estimates we can calculate the resulting uncertainty in calculating U_p.

Figure 2 shows an explicit example of the timing calculations for one of the 10 selected 1-D SSMHs, with Figures 2a and 2e for a significant drop in the magnetic field magnitude from about 3.0 nT to 0.5 nT (in about 10 s for the leading boundary). Figures 2a–2d are for the leading boundary, and Figures 2e–2h are for the trailing. The four horizontal lines represent four different selected cuts chosen to calculate the timing velocity. Namely, we calculate the timing velocity at those four different positions. In Figure 2b, the average velocity of the leading boundary in the satellite frame is 66.6 km/s and the average standard deviation is $\sigma = 3.8$ km/s, where the averages are taken over U1–U4 and $\sigma 1$–$\sigma 4$, respectively. From Figures 2c and 2d, we can see that the mean velocity of the leading boundary in the plasma flow frame is $U_p = (30.9 \pm 5.2)$ km/s along the normal $\vec{\mathbf{n}} = (0.08, -0.65, -0.75)$. The average background plasma flow velocity in GSE is (22, 0.5, −46) km/s during the time interval 22:14:48 to 22:15:48. Figures 2e–2h are for the trailing boundary. In the plasma flow frame of trailing boundary, propagation speed is (39.2 ± 5.5) km/s along the normal $\vec{\mathbf{n}} = (0.06, -0.76, -0.65)$ with an uncertainty of 6°. To ensure the reliability, different components and resolutions of magnetic field data are used in calculating the timing velocity. The results show a good agreement with that in Figure 2. The velocity in the plasma frame is nonzero, clearly demonstrating a structure propagation in the plasma flow frame. Also, among the 10 events well suited for the timing method, there are 8 such SSMHs propagation events. And a statistical work is shown as follows in subsection 3.3 and section 4 with the possible mechanism is discussed.

3.2. MDD and STD Analysis

The MDD and STD methods are also used to calculate the timing velocity and the normal in this study. As we mentioned, the MDD method can analyze the dimensionality character of observed structures. The technique provides three directions of maximum, minimum, and intermediate variations in the magnetic field. With the STD method the velocity of the observed structure can be calculated. Using the MDD and STD methods on

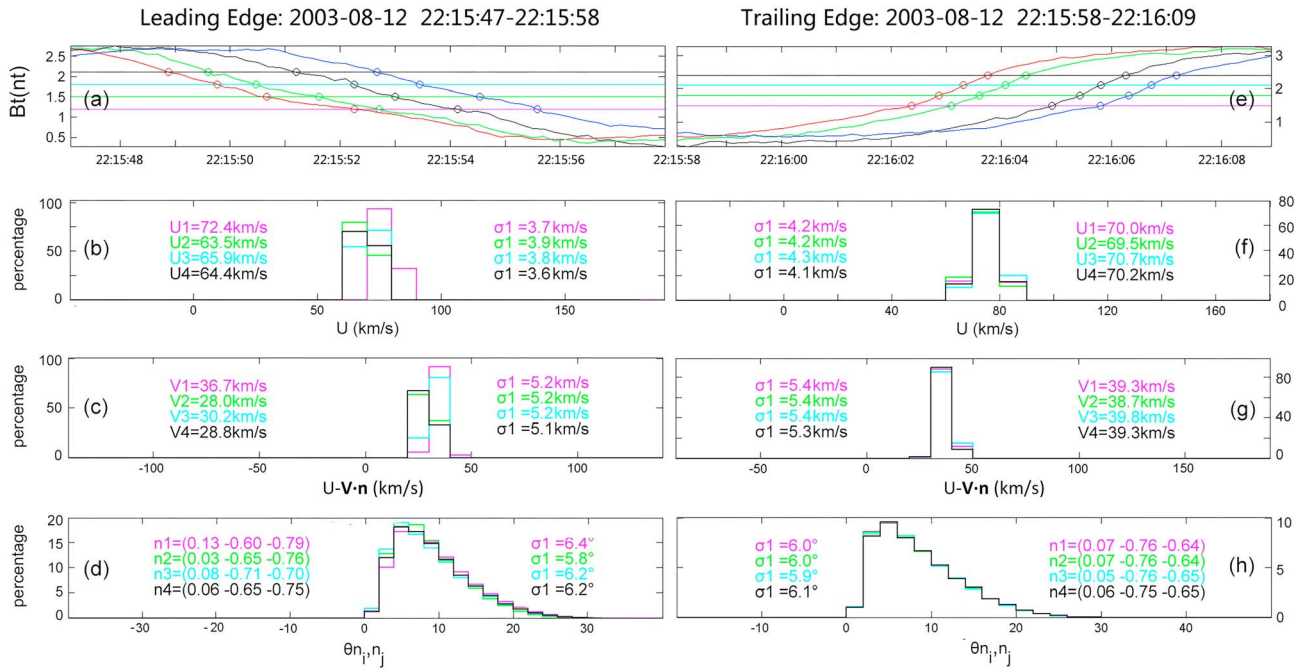

Figure 2. Timing analysis for a representative event: The timing analysis results for the (a–d) leading and (e–h) trailing boundaries, respectively. The horizontal color lines in Figures 2a and 2e are for the moments when the four spacecraft cross the event, corresponding to the histogram of the same color in Figures 2b–2d and 2f–2h. The magnetic field in GSE coordinates (Figures 2a and 2e). Histograms of the velocities in the satellite frame, with U1–U4 are the average velocities and $\sigma 1$–$\sigma 4$ are their standard deviations (Figures 2b and 2f). The vertical axis is the percentage of all the 11^3 values in each bin for one calculation. Histograms of the velocities in the plasma flow frame (Figures 2c and 2g). Histograms of angles between any two normal vectors (Figures 2d and 2h).

the example in Figure 2, we obtain results shown in Figure 3. For the dimensionality, the MDD method suggests that a structure can be considered quasi-1D if $\lambda_1 >> \lambda_2$ and λ_3, where λ_1 is the eigenvalue for the direction of maximum variation of the magnetic field and therefore also the normal of the MH boundary. For the leading boundary from 22:15:51 to 22:15:56, the blue region in Figure 3, we find that $\lambda_1 >> \lambda_2$ and λ_3 with an average ratio of λ_1, λ_2, and λ_3 as 84:13:1. Similarly, the average ratio of the three eigenvalues for

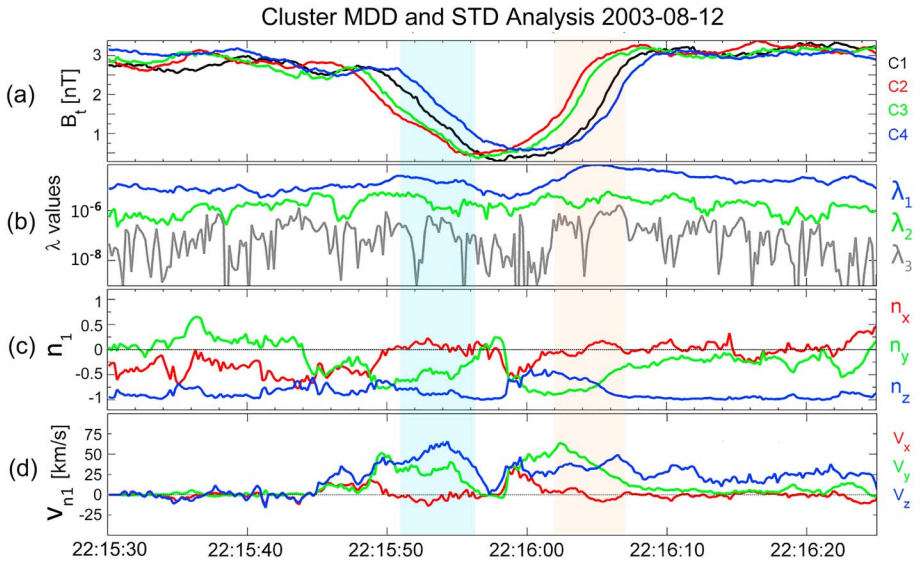

Figure 3. (a) Cluster (C1–C4) observations of the magnetic field in GSE coordinates; (b) eigenvalues λ_1, λ_2, and λ_3; (c) the maximum derivative direction of the magnetic field calculated at every moment; and (d) velocities along the maximum direction calculated at every moment. The data in the blue and yellow regions are used to calculate the average λ, $\mathbf{n}_1$, and velocities of the leading and trailing boundaries, respectively.

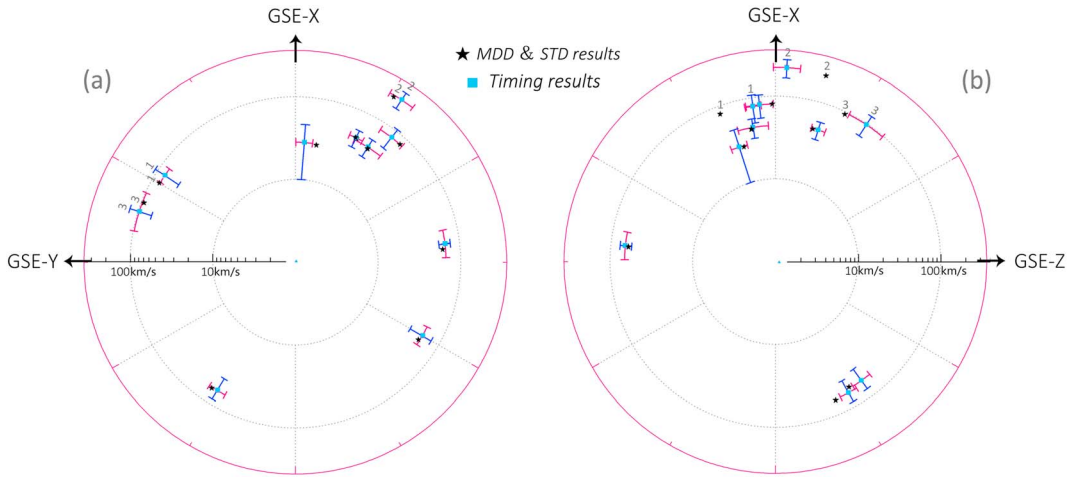

Figure 4. Timing, MDD, and STD analysis results with azure squares and black asterisks corresponding to the timing and MDD + STD analysis, respectively. The results in the (a) GSE XY and (b) GSE XZ planes, with the radius for the velocity magnitude and the positioning angles for the velocity direction. Error bars are from the timing analysis. Three events have a small deviation are marked as "1, 2, and 3". To make the blue error bars clearer, they are shown 5 times of the real values.

the trailing boundary (the yellow region) is 96:6:1. Thus, this event can be regarded as a quasi-1D structure with the validity of the timing method.

Figures 3c and 3d show the maximum variation direction $\mathbf{n}_1$ and the structure velocity along $\mathbf{n}_1$. The mean direction and velocity of leading and trailing boundaries over these periods are $\mathbf{n}_L = (0.07, -0.62, -0.78)$, $U_L = 61.2$ km/s, $\mathbf{n}_T = (0.09, -0.77, -0.63)$, and $U_T = 57.2$ km/s, respectively. The results show a good agreement with the timing results above. We also project the leading boundary velocity vector (obtained from the MDD and STD methods) onto the trailing boundary velocity vector and find the difference between the two is less than 5 km/s. Thus, the event in Figure 3 can be considered a "stable" structure as defined in *Xiao et al*. [2015].

By combining the results of the MDD and STD methods with the background plasma flow used for the timing results, we obtain the propagating velocity in the plasma flow for the example event, 30.3 km/s and 34.3 km/s of the leading and trailing boundaries, respectively.

3.3. Statistical Results

In Figure 4 the velocity magnitude and direction in the spacecraft reference frame in the GSE-XY and GSE-XZ planes are shown by the timing, MDD, and STD analysis for the 10 quasi-1D events. We find that the timing analysis accord well with the MDD and STD results in the GSE-XY plane with the difference between the obtained normal directions is less than 5°. Also in the GSE-XZ plane, most results agree well with each other, except for three events where the normal directions have a small deviation (mark as "1, 2, and 3") of $<7°$. Therefore, the timing analysis is in agreement with the MDD and STD results for the majority of the events. In addition, we find that the events have a propagation velocity toward to the Earth in the spacecraft reference frame. This will be a topic of future studies.

4. Possible Mechanisms

Tsurutani et al. [2011] suggested alternative approaches rather than the mirror mode for the generation mechanism of magnetic dips. Indeed, for the 1-D events investigated in this study, we find them in a mirror stable environment [*Sun et al*., 2012]. We also check the spatial scale of the events by multiplying the observed duration and the timing velocity. We find that the scale size of these magnetic holes is less than or close to the proton Larmor radii (ρ_i) (from $0.3\,\rho_i$ to $1.5\,\rho_i$). The physical mechanism of the mirror-mode instability is based on the adiabatic reflection of particles in a temporally varied nonuniform magnetic field background; and thus, the scale of the unstable mirror mode should substantially exceed the ion gyroradius. Therefore, it is not appropriate for explaining small-scale structures. For 2-D SSMHs, their formation is primarily associated with other mechanisms, such as electron vortices [*Haynes et al*., 2015]. In addition, a tearing mode mechanism has been

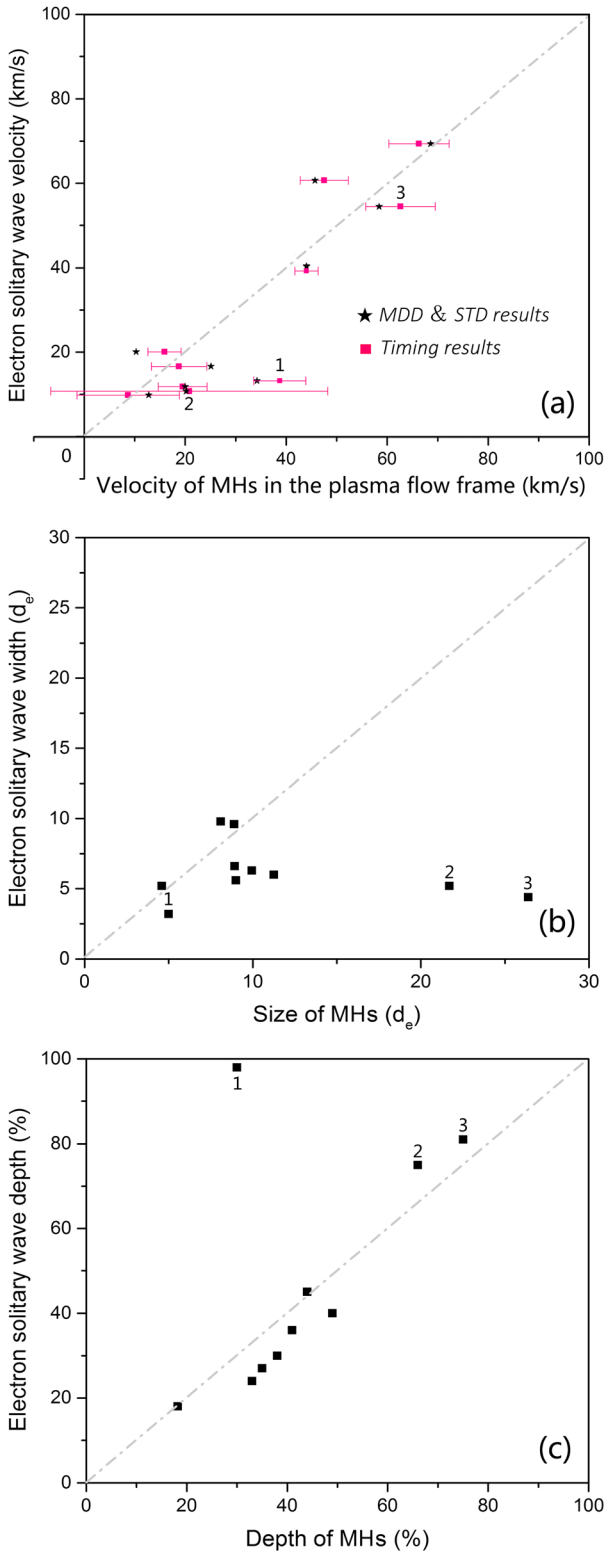

used to explain the events observed in an active magnetotail. *Balikhin et al.* [2012] have suggested that in an active magnetotail a localized region of the cross-tail current sheet could become unstable and exciting tearing mode instability, which could explain the events reported by *Ge et al.* [2011]. However, the events studied in the present study were measured during quiet geomagnetic conditions. Hence, the tearing mode does not adapt to explain these observations. On the other hand, nonlinear kinetic Alfvén waves (KAW) can also produce substantial localized magnetic disturbances with a transverse scale of the ion gyroradius. However, comparing the local Alfvén speed with the MH propagation velocity in the events studied, we find an order of magnitude difference between them. Particularly, for the typical KAW with a significant k_{perp} (the transverse scale) effect, e.g., a parallel phase velocity about 50% higher than the local Alfvén speed [*Baumjohann and Treumann*, 1996], the KAW phase velocities are 12–23 times higher than the propagating velocity of MHs. Furthermore, it is found that the magnetic field perturbations of these MHs are in the direction parallel, not transverse, to the background magnetic field (B_{bg}) and propagate perpendicularly to B_{bg}. Take the case in Figure 1, for example, the angle between the total magnetic field perturbation (~80% of B_{bg}) and B_{bg} is about 170°, and the angle between the propagating velocities and B_{bg} is about 99°. These features are inconsistent with the nonlinear KAW.

Also, the slow-mode electron solitary wave can be considered a possible candidate for the generation of 1-D SSMHs. Based on *Ji et al.* [2014], we use Cluster PEACE data to estimate the velocity of SSMHs by the solitary

Figure 5. (a) Electron solitary wave velocity in EMHD model versus SSMHs propagating velocity calculated in the background plasma flow frame. The horizontal axis denotes the timing/MDD + STD velocity in the plasma flow frame, while the vertical axis represents the electron solitary wave velocity by the theoretical model with its typical parameters from data average. (b) The observed size of MHs in comparison with calculated soliton widths. (**c**) The observed depth of MHs in comparison with calculated values. The equality line is marked by the dash-dotted line, and three off fit events are marked as 1, 2, and 3.

wave velocity of $d_e V_{Ae}\mathbf{K_N}$, where d_e is the electron skin depth, V_{Ae} is the electron Alfvén velocity, and $\mathbf{K_N}$ is the typical variation length of the electron density [*Ji et al*., 2014]. The calculation process is as follows for an example event detected by Cluster in the period of 14:30:50 UT to 14:31:10 UT in July 2003, with $d_e = 64.31$ km, $V_{Ae} = 342$ km/s, and $\mathbf{K_N} = (-9.26, -9.25, -12.2)\ 10^{-4}\,\mathrm{km}^{-1}$. Applying the typical parameters of $n_e = 0.27\,\mathrm{cm}^{-3}$ and Bt = 8.1 nT, the background electron number density and magnetic field magnitude averaged over C1–C4 data over 1 min, we can obtain d_e and V_{Ae}. We also use $G_{ne} = (-2.5, -2.4, -3.3)\ 10^{-4}\,\mathrm{cm}^3/\mathrm{km}$ to obtain $\mathbf{K_N}$, where G_{ne} is the 1 min average electron density gradient calculated by the position and electron number density differences between C1 and C4. Then the electron solitary wave velocity is calculated 39.0 km/s for this event. We compare this result with the timing and MDD and STD analysis of 44.1 km/s and 46.2 km/s, respectively, and find that they are in a good agreement.

Figure 5a shows a comparison between the theoretical estimate of the electron solitary wave velocity and the observed velocity (from the timing, MDD, and STD methods) of SSMHs in the background plasma flow for all 10 events we selected. If the error bar for an event goes through or approaches to the vertical axis, we consider that this event may be frozen in the plasma flow. Thus, in this figure we can see eight events are propagating in the plasma flow frame and two events may be frozen in it. There is only a single event, however, with a large error, possibly due to the fact that this event is observed within a high speed plasma flow (300–350 km/s).

As we know, mirror modes are nonpropagating structures in the space plasma environment [e.g., *Hasegawa*, 1969; *Southwood and Kivelson*, 1993]. Therefore, these propagating events in this paper are clearly different from the mirror modes. From Figure 5a we find a good agreement between the electron solitary wave velocity and the SSMHs propagation in the background plasma flow obtained with the timing, MDD, and STD methods. Also, the velocity of the soliton is related with its amplitude and size. *Ji et al*. [2014] and *Li et al*. [2016] have calculated the depth and width from the propagating velocity by EMHD solitary wave model and found the results are in agreements with the observations. Here we again analyze the event in the period of 14:30:50 UT to 14:31:10 UT in July 2003 to show the relation between the observed magnetic holes and the electron solitary waves. In the event, the depth of the MH is $D \approx 49\%$, and the MH scale is $L = 600\,\mathrm{km} \approx 9\,d_e$. By using the soliton solution in *Ji et al*. [2014], equation (15), or *Li et al*. [2016], equation (5), we obtain the soliton width $L = 2d_e\sqrt{\frac{\widetilde{V}}{V_0 - V}}$ and depth $D = 3(V_0 - \widetilde{V})$, where V_0 and $\widetilde{V}$ are the observed propagating velocity and slow-mode velocity normalized by $d_e V_{Ae}\mathbf{K_N}$, respectively. Then we get the theoretical soliton depth $D \approx 40\%$ and $L \approx 5.6\,d_e$ with $V_0 = 1.13$ and $\widetilde{V} = 1$. This indicates the theoretical depth and width of a soliton are on the same order with the observed magnetic hole. In Figures 5b and 5c, the observed width and depth of the 10 discussed MHs are compared with the calculated results by substituting the observed parameters, d_e, V_0, and $\widetilde{V}$ into the EMHD soliton width $L = 2d_e\sqrt{\frac{\widetilde{V}}{V_0 - V}}$ and depth $D = 3(V_0 - \widetilde{V})$. It is found that there are seven events in which the results match each other well. They are clearly EMHD solitons. The other three events with an off fit are marked as 1, 2, and 3, due to a fast MH velocity (almost twice the theoretical prediction as shown in Figure 5a) for Event 1 and bigger observed MH widths in Events 2 and 3. Even for the off cases, the width is fitted well for Event 1 while the depth is fitted well for Events 2 and 3. Therefore, the EMHD soliton wave is very likely a possible candidate for the formation of these propagating MHs. Thus, we suggest that the electron solitary wave is a possible mechanism for generating these propagating events. Still, more work should be done to study it furthermore.

5. Summary

We have calculated the velocity of SSMHs detected by Cluster (C1–C4) in the plasma sheet from July 2003 to October 2003. The timing, MDD, and STD methods are used to determine the normal direction and velocity of the structures in the satellite frame. Based on the results, the velocity of the SSMHs in the background plasma flow frame has been obtained. Also, several measures have been done to ensure the results as shown in section 2 and 3. It is found that 8 of the 10 events are clearly propagating SSMHs in the plasma flow. By the model of *Ji et al*. [2014], we calculate the solitary wave velocity, width, and depth from Cluster data; 7 of the 10 events are in a good agreement with the observations of SSMHs. Therefore, we suggest that the electron solitary wave should be a possible mechanism for SSMHs.

Acknowledgments
We are very grateful to the instrumental teams of Cluster FGM (PI: Elisabeth Lucek), CIS (PI: Iannis Dandouras), and PEACE (PI: Andrew Fazakerley) for providing magnetic field and plasma data. All Cluster data can be obtained from the Cluster Science Archive (http://www.cosmos.esa.int/web/csa/). This work was supported by the National Natural Science Foundation of China (grants 41322031 and 41574157), and the SNSB grant 77/14.

References

Balikhin, M. A., D. G. Sibeck, A. Runov, and S. N. Walker (2012), Magnetic holes in the vicinity of dipolarization fronts: Mirror or tearing structures, *J. Geophys. Res.*, *117*, A08229, doi:10.1029/2012JA017552.

Balogh, A., et al. (2001), The Cluster magnetic field investigation: Overview of in-flight performance and initial results, *Ann. Geophys.*, *19*, 1207–1217, doi:10.5194/angeo-19-1207-2001.

Basu, B., and B. Coppi (1982), Field-swelling instability in anisotropic plasmas, *Phys. Rev. Lett.*, *48*, 799, doi:10.1103/PhysRevLett.48.799.

Baumgärtel, K. (1999), Soliton approach to magnetic holes, *J. Geophys. Res.*, *104*, 28,295–28,308, doi:10.1029/1999JA900393.

Baumjohann, W., and R. A. Treumann (1996), *Basic Space Plasma Physics*, pp. 247–283, Imperial Coll. Press, London.

Biermann, L. (1950), Über den Ursprung der Magnetfelder auf Sternen und im interstellaren Raum, *Z. Naturforsch., A: Phys. Sci.*, *5*, 65–71.

Burlaga, L. F., and J. F. Lemaire (1978), Interplanetary magnetic holes: Theory, *J. Geophys. Res.*, *83*, 5157–5160, doi:10.1029/JA083iA11p05157.

Chisham, G., S. J. Schwartz, M. A. Balikhin, and M. W. Dunlop (1999), AMPTE observations of mirror mode waves in the magnetosheath: Wavevector determination, *J. Geophys. Res.*, *104*, 437–447, doi:10.1029/1998JA900044.

Denton, R. E., B. U. Ö. Sonnerup, J. Birn, W.-. L. Teh, J. F. Drake, M. Swisdak, M. Hesse, and W. Baumjohann (2010), Test of methods to infer the magnetic reconnection geometry from spacecraft data, *J. Geophys. Res.*, *115*, A10242, doi:10.1029/2010JA015420.

Denton, R. E., B. U. Ö. Sonnerup, M. Swisdak, J. Birn, J. F. Drake, and M. Hesse (2012), Test of Shi et al. method to infer the magnetic reconnection geometry from spacecraft data: MHD simulation with guide field and antiparallel kinetic simulation, *J. Geophys. Res.*, *117*, A09201, doi:10.1029/2012JA017877.

Fazakerley, A. N., and D. J. Southwood (1994), Theory and observation of magnetosheath waves, in *Solar Wind Sources of Magnetosheath Ultra- Low-Frequency Waves*, *Geophys. Monogr. Ser.*, vol. 81, edited by M. Engebretson, K. Takahashi, and M. Scholer, pp. 147–158, AGU, Washington, D. C.

Gary, S. P., and H. Karimabadi (2006), Linear theory of electron temperature anisotropy instabilities: Whistler, mirror, and Weibel, *J. Geophys. Res.*, *111*, A11224, doi:10.1029/2006JA011764.

Ge, Y. S., J. P. McFadden, J. Raeder, V. Angelopoulos, D. Larson, and O. D. Constantinescu (2011), Case studies of mirror-mode structures observed by THEMIS in the near-Earth tail during substorms, *J. Geophys. Res.*, *116*, A01209, doi:10.1029/2010JA015546.

Hasegawa, A. (1969), Drift mirror instability in the magnetosphere, *Phys. Fluids*, *12*, 2642–2650, doi:10.1063/1.1692407.

Haynes, C. T., D. Burgess, E. Camporeale, and T. Sundberg (2015), Electron vortex magnetic holes: A nonlinear coherent plasma structure, *Phys. Plasmas*, *22* 012309, doi:10.1063/1.4906356.

Horbury, T. S., E. A. Lucek, A. Balogh, I. Dandouras, and H. Rème (2004), Motion and orientation of magnetic field dips and peaks in the terrestrial magnetosheath, *J. Geophys. Res.*, *109*, A09209, doi:10.1029/2003JA010237.

Ji, X.-F. (2015), Magnetohydrodynamics solitons on multiple scales as possible mechanisms for observed magnetic holes PhD thesis, Peking Univ., China.

Ji, X.-F., X.-G. Wang, W.-J. Sun, C.-J. Xiao, Q.-Q. Shi, J. Liu, and Z.-Y. Pu (2014), EMHD theory and observations of electron solitary waves in magnetotail plasmas, *J. Geophys. Res. Space Physics*, *119*, 4281–4289, doi:10.1002/2014JA019924.

Johnstone, A. D., et al. (1997), PEACE: A Plasma Electron And Current Experiment, *Space Sci. Rev.*, *79*, 351–398, doi:10.1023/A:1004938001388.

Joy, S. P., M. G. Kivelson, R. J. Walker, K. K. Khurana, C. T. Russell, and W. R. Paterson (2006), Mirror-mode structures in the Jovian magnetosheath, *J. Geophys. Res.*, *111*, A12212, doi:10.1029/2006JA011985.

Kaufmann, R. L., J.-T. Horng, and A. Wolfe (1970), Large-amplitude hydromagnetic waves in the inner magnetosheath, *J. Geophys. Res.*, *75*(25), 4666–4676, doi:10.1029/JA075i025p04666.

Knetter, T. (2005), A new perspective of the solar wind micro-structure due to multi-point observations of discontinuities PhD thesis, Univ. zu Köln.

Knetter, T., F. M. Neubauer, T. Horbury, and A. Balogh (2004), Four-point discontinuity observations using Cluster magnetic field data: A statistical survey, *J. Geophys. Res.*, *109*, A06102, doi:10.1029/2003JA010099.

Li, Z.-Y., W.-J. Sun, X.-G. Wang, Q.-Q. Shi, C.-J. Xiao, Z.-Y. Pu, X.-F. Ji, S.-T. Yao, and S.-Y. Fu (2016), An EMHD soliton model for small-scale magnetic holes in magnetospheric plasmas, *J. Geophys. Res. Space Physics*, *121*, doi:10.1002/2016JA022424.

Paschmann, G., A. N. Fazakerley, and S. J. Schwartz (1998), Moments of plasma velocity distributions, in *Analysis Methods for Multi-Spacecraft Data*, pp. 125–158, ISSI SA Publications Division, Noordwijk, Netherlands.

Pokhotelov, O. A., O. G. Onishchenko, and L. Stenflo (2013), Physical mechanisms for electron mirror and field swelling modes, *Phys. Scr.*, *87*(6065303), doi:10.1088/0031-8949/87/06/065303.

Rème, H., et al. (2001), First multispacecraft ion measurements in and near the Earth's magnetosphere with the identical Cluster ion spectrometry (CIS) experiment, *Ann. Geophys.*, *19*, 1303–1354, doi:10.5194/angeo-19-1303-2001.

Russell, C. T., M. M. Mellott, E. J. Smith, and J. H. King (1983), Multiple spacecraft observations of interplanetary shocks: Four spacecraft determination of shock normals, *J. Geophys. Res.*, *88*(A6), 4739–4748, doi:10.1029/JA088iA06p04739.

Schwartz, S. J. (1998), Shock and discontinuity normals, Mach numbers, and related parameters, in *Analysis Methods for Multi-Spacecraft Data, Report*, edited by G. Paschmann and P. W. Daly, pp. 249–270, International Space Science Institute ISSI, Bern, Switz.

Shi, Q. Q., C. Shen, Z. Y. Pu, M. W. Dunlop, Q.-G. Zong, H. Zhang, C. J. Xiao, Z. X. Liu, and A. Balogh (2005), Dimensional analysis of observed structures using multipoint magnetic field measurements: Application to Cluster, *Geophys. Res. Lett.*, *32*, L12105, doi:10.1029/2005GL022454.

Shi, Q. Q., C. Shen, M. W. Dunlop, Z. Y. Pu, Q.-G. Zong, Z. X. Liu, E. Lucek, and A. Balogh (2006), Motion of observed structures calculated from multi-point magnetic field measurements: Application to Cluster, *Geophys. Res. Lett.*, *33*, L08109, doi:10.1029/2005GL025073.

Shi, Q. Q., et al. (2009a), Spatial structures of magnetic depression in the Earth's high-altitude cusp: Cluster multipoint observations, *J. Geophys. Res.*, *114*, A10202, doi:10.1029/2009JA014283.

Shi, Q. Q., et al. (2009b), Cluster observations of the entry layer equatorward of the cusp under northward interplanetary magnetic field, *J. Geophys. Res.*, *114*, A12219, doi:10.1029/2009JA014475.

Shi, Q. Q., et al. (2013), Solar wind entry into the high-latitude terrestrial magnetosphere during geomagnetically quiet times, *Nat. Commun.*, *4*, 1466, doi:10.1038/ncomms2476.

Southwood, D. J., and M. G. Kivelson (1993), Mirror instability: 1. Physical mechanism of linear instability, *J. Geophys. Res.*, *98*(A6), 9181–9187, doi:10.1029/92JA02837.

Stasiewicz, K. (2004), Theory and observations of slow-mode solitons in space plasmas, *Phys. Rev. Lett.*, *93* 125004, doi:10.1103/PhysRevLett.93.125004.

Stasiewicz, K., P. K. Shukla, G. Gustafsson, S. Buchert, B. Lavraud, B. Thidé, and Z. Klos (2003), Slow magnetosonic solitons detected by the Cluster spacecraft, *Phys. Rev. Lett.*, *90* 085002, doi:10.1103/PhysRevLett.90.085002.

Sun, W. J., et al. (2010), Statistical research on the motion properties of the magnetotail current sheet: Cluster observations, *Sci. China Tech. Sci.*, *53*, 1732–1738, doi:10.1007/s11431-010-3153-y.

Sun, W. J., et al. (2012), Cluster and TC-1 observation of magnetic holes in the plasma sheet, *Ann. Geophys.*, *30*, 583–595, doi:10.5194/angeo-30-583-2012.

Sundberg, T., D. Burgess, and C. T. Haynes (2015), Properties and origin of subproton-scale magnetic holes in the terrestrial plasma sheet, *J. Geophys. Res. Space Physics*, *120*, 2600–2615, doi:10.1002/2014JA020856.

Tsurutani, B. T., E. Smith, R. Anderson, K. Ogilvie, J. Scudder, D. Baker, and S. Bame (1982), Lion roars and nonoscillatory drift mirror waves in the magnetosheath, *J. Geophys. Res.*, *87*(A8), 6060–6072, doi:10.1029/JA087iA08p06060.

Tsurutani, B. T., F. L. Guarnieri, E. Echer, G. S. Lakhina, and O. P. Verkhoglyadova (2009), Magnetic decrease formation from $<$1 AU to 5 AU: Corotating interaction region reverse shocks, *J. Geophys. Res.*, *114*, A08105, doi:10.1029/2008JA013927.

Tsurutani, B. T., G. S. Lakhina, O. P. Verkhoglyadova, E. Echer, F. L. Guarnieri, Y. Narita, and D. O. Constantinescu (2011), Magnetosheath and heliosheath mirror mode structures, interplanetary magnetic decreases, and linear magnetic decreases: Differences and distinguishing features, *J. Geophys. Res.*, *116*, A02103, doi:10.1029/2010JA015913.

Turner, J. M., L. F. Burlaga, N. F. Ness, and J. F. Lemaire (1977), Magnetic holes in the solar wind, *J. Geophys. Res.*, *82*, 1921–1924, doi:10.1029/JA082i013p01921.

Wendel, D. E., and M. L. Adrian (2013), Current structure and nonideal behavior at magnetic null points in the turbulent magnetosheath, *J. Geophys. Res. Space Physics*, *118*, 1571–1588, doi:10.1002/jgra.50234.

Winterhalter, D., M. Neugebauer, B. E. Goldstein, E. J. Smith, S. J. Bame, and A. Balogh (1994), Ulysses field and plasma observations of magnetic holes in the solar wind and their relation to mirror-mode structures, *J. Geophys. Res.*, *99*, 23,371–23,381, doi:10.1029/94JA01977.

Xiao, T., et al. (2010), Cluster-C1 observations on the geometrical structure of linear magnetic holes in the solar wind at 1 AU, *Ann. Geophys.*, *28*, 1695–1702, doi:10.5194/angeo-28-1695-2010.

Xiao, T., Q. Q. Shi, and W. J. Sun (2011), Cluster observations of magnetic holes near the interplanetary current sheets at 1 AU, in *2011 30th URSI Gen. Ass. Sci. Symp.*, pp. 1–3.

Xiao, T., Q. Q. Shi, A. M. Tian, W. J. Sun, H. Zhang, X. C. Shen, and A. M. Du (2014), Plasma and magnetic-field characteristics of magnetic decreases in the solar wind at 1 AU: Cluster-C1 observations, *Sol. Phys.*, *289*(8), 3175–3195, doi:10.1007/s11207-014-0521-y.

Xiao, T., et al. (2015), Propagation characteristics of young hot flow anomalies near the bow shock: Cluster observations, *J. Geophys. Res. Space Physics*, *120*, 4142–4154, doi:10.1002/2015JA021013.

Zhang, T. L., et al. (2008), Characteristic size and shape of the mirror mode structures in the solar wind at 0.72 AU, *Geophys. Res. Lett.*, *35*, L10106, doi:10.1029/2008GL033793.

Zhang, T. L., W. Baumjohann, C. T. Russell, L. K. Jian, C. Wang, J. B. Cao, M. Balikhin, X. Blanco-Cano, M. Delva, and M. Volwerk (2009), Mirror mode structures in the solar wind at 0.72 AU, *J. Geophys. Res.*, *114*, A10107, doi:10.1029/2009JA014103.